

# Tests of the Monte Carlo Simulation of the Photon-Tagger Focal-Plane Electronics at the MAX IV Laboratory

M.F. Preston<sup>a</sup>, L.S. Myers<sup>b,1</sup>, J.R.M. Annand<sup>c</sup>, K.G. Fissum<sup>a,\*</sup>, K. Hansen<sup>e</sup>,  
L. Isaksson<sup>e</sup>, R. Jebali<sup>d,2</sup>, M. Lundin<sup>e</sup>

<sup>a</sup>*Lund University, SE-221 00 Lund, Sweden*

<sup>b</sup>*Duke University, Durham NC 27708, USA*

<sup>c</sup>*University of Glasgow, Glasgow G12 8QQ, Scotland, UK*

<sup>d</sup>*Arktis Radiation Detectors Limited, 8045 Zürich, Switzerland*

<sup>e</sup>*MAX IV Laboratory, Lund University, SE-221 00 Lund, Sweden*

---

## Abstract

Rate-dependent effects in the electronics used to instrument the tagger focal plane at the MAX IV Laboratory were recently investigated using the novel approach of Monte Carlo simulation to allow for normalization of high-rate experimental data acquired with single-hit time-to-digital converters (TDCs). The instrumentation of the tagger focal plane has now been expanded to include multi-hit TDCs. The agreement between results obtained from data taken using single-hit and multi-hit TDCs demonstrate a thorough understanding of the behavior of the detector system.

*Keywords:* tagger hodoscope, rate dependencies, multi-hit time-to-digital converters

---

## 1. Introduction

The Tagged-Photon Facility (TPF) [1, 2] at the MAX IV Laboratory [3] in Lund, Sweden has been used to measure photonuclear cross sections in many experiments. Rate-dependent deadtime and other effects in the electronics used to instrument the tagger focal plane (FP) must be correctly addressed in order to properly normalize the experimental data. These effects are particularly important because of the intermittently high instantaneous photon-beam flux caused by the non-uniform time structure of the photon beam. Limitations in

---

\*Corresponding author. Telephone: +46 46 222 9677; Fax: +46 46 222 4709

*Email address:* kevin.fissum@nuclear.lu.se (K.G. Fissum)

<sup>1</sup>present address: Thomas Jefferson National Accelerator Facility, Newport News VA 23606, USA

<sup>2</sup>present address: University of Glasgow, Glasgow G12 8QQ, Scotland, UK

the FP instrumentation electronics were also problematic. An in-depth investigation of the rate-dependent effects at the TPF was recently reported [4] in which the novel approach of Monte Carlo simulation was employed. The behavior of the FP instrumentation electronics was successfully modeled for each detected electron in 1 ns steps. Input parameters were taken directly from the electronics setup (such as pulse widths) or from the data itself (such as electron rates and time structure of the electron beam).

The major limitation in the original electronic instrumentation system for the FP which led to large corrections at high rates was the use of single-hit time-to-digital converters (TDCs). These TDCs were used to measure the elapsed time between a photon-induced reaction product and the post-bremsstrahlung electron corresponding to the photon in question. Understanding the behavior of the single-hit TDCs at high rates has enabled the absolute normalization of data [5]. Recently, the instrumentation of the tagger FP has been upgraded to include multi-hit TDCs; that is, TDCs which are sensitive to more than one stop signal they receive when triggered. Such TDCs are superior to their single-hit predecessors as the data they provide eliminate the need for a large rate-dependent correction to the absolute experiment normalization (see below). This in turn simplifies the data analysis.

In this paper, we present a detailed analysis of the behavior of the tagger FP instrumented with multi-hit TDCs. We compare this behavior to that of the tagger FP instrumented with single-hit TDCs and demonstrate good agreement. Finally, we present absolute cross-section data obtained using both devices and compare it to existing data to demonstrate a thorough understanding of the behavior of the detector system.

## 2. Facility overview

At the TPF, photon taggers [6–8] and the well-known photon-tagging technique [1, 9, 10] (see Fig. 1) are used to perform photonuclear investigations. A pulse-stretched electron beam [11] with an energy of up to 200 MeV is used to produce bremsstrahlung as it passes through a  $\sim 100 \mu\text{m}$  Al radiator. The resulting bremsstrahlung photon beam is collimated prior to striking the experimental target. Post-bremsstrahlung electrons are momentum-analyzed in the tagging spectrometer equipped with a 63-detector plastic-scintillator array positioned at the focal plane. A prompt coincidence between a photonuclear reaction product and a post-bremsstrahlung electron in the scintillator array indicates a tagged-photon event.

The energy of the tagged photon is determined from the difference between the energy of the incident electron beam and the energy of the post-bremsstrahlung electron detected in the scintillator focal plane (FP). The measured cross section is given by

$$\frac{d\sigma}{d\Omega} = \frac{Y_{\text{coincidence}}/\epsilon_{\text{detector}}}{N_{\text{target}} \cdot N_{\text{electrons}} \cdot \epsilon_{\text{tagg}} \cdot \Delta\Omega}, \quad (1)$$

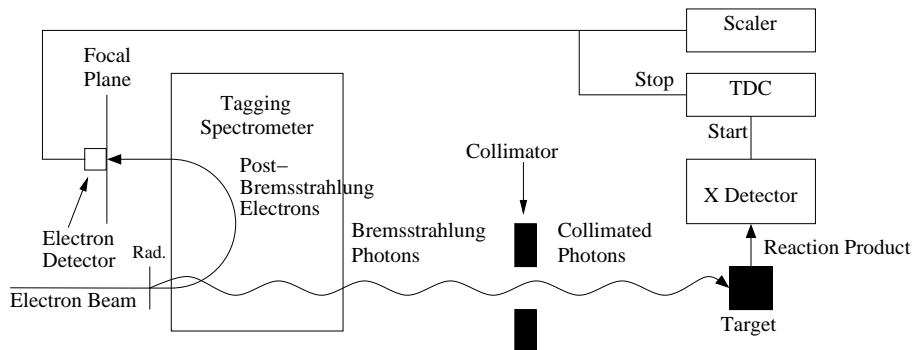


Figure 1: The photon-tagging technique. Beam electrons may radiate bremsstrahlung photons. Post-bremsstrahlung electrons are momentum analyzed using a photon tagger. Bremsstrahlung photons which pass through the collimator to strike the target and may induce photonuclear reactions. The coincidence between a reaction product and a post-bremsstrahlung electron is a tagged-photon event. Figure from [4].

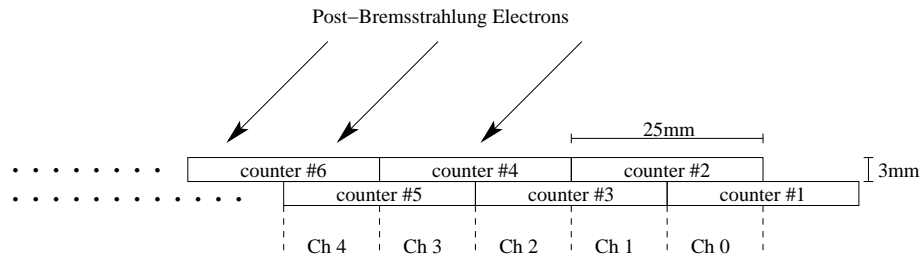


Figure 2: The FP hodoscope in 50%-overlap configuration. A coincidence between a detector in the front plane and a detector in the back plane defines a tagger channel. There are a total of 63 detectors and thus 62 channels in the FP. Figure from [4].

where  $Y_{\text{coincidence}}$  is the number of true, prompt coincidences between the reaction-product detector and the FP,  $\epsilon_{\text{detector}}$  is the reaction-product detector efficiency,  $N_{\text{target}}$  is the number of target nuclei per unit area,  $N_{\text{electrons}}$  is the number of electrons detected in the FP array and counted in the FP scalars,  $\epsilon_{\text{tagg}}$  is the probability that a taggable bremsstrahlung photon passes through the beam-defining collimator and hits the target [1], and  $\Delta\Omega$  is the solid angle subtended by the reaction-product detector. Both  $Y_{\text{coincidence}}$  and  $N_{\text{electrons}}$  must be corrected for the effects of deadtime in the instrumentation electronics, and the size of the corrections depends on the count rate. This is complicated by the fact that the electron beam delivered by the accelerator has a periodic structure of varying intensity. As a result, the instantaneous FP rate can be almost a factor of 4 higher than the average FP rate (typically 3 MHz/MeV) at 20 nA, a typical average operating current.

The FP hodoscope consists of two parallel rows of NE110 scintillators. The front row nearest the exit window of the tagger magnet has 31 elements, while the back row has 32 elements (see Fig. 2). The signals from the detectors are

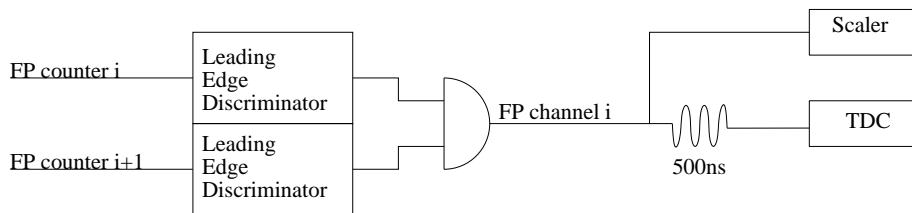


Figure 3: The FP electronics. A coincidence between an electron-detector signal in the front plane of the FP and an electron-detector signal in the back plane of the FP defines a tagger channel. The coincidence module looking for these overlaps was from SAL. This signal was counted and used to stop a TDC started by the photonuclear reaction-product detector.

passed to LRS 4413 leading-edge discriminators operated in burst-guard mode. The resulting logic signals are typically set to 25 or 50 ns. Overlap coincidence modules designed and built at the Saskatchewan Accelerator Laboratory (SAL) are used to identify coincidences between two physically overlapping detectors in the front and back rows. An output pulse is generated whenever the two input pulses overlap and is ended whenever one or both inputs are reset. An overlap of at least 3 ns is necessary to produce an output pulse. These coincidences define FP channels and are used to stop TDCs and increment scalars. When a post-bremsstrahlung electron event occurs in coincidence with a trigger from the experiment detectors, a tagged-photon event may have occurred.

The device labeled TDC in Figs. 1 and 3 represents both single-hit and multi-hit TDCs – that is, both devices are used in parallel – started by the same signal and stopped by the same signal(s). The single-hit TDC used to instrument the FP array is the CAEN V775. The V775 is a 32 channel device with 12 bit resolution. It is operated in common-start mode. The stop comes from the first signal presented by a FP channel. It was experimentally determined that to be registered by the TDC, the stop signals corresponding to a FP channel had to correspond to a timing overlap of at least  $\sim 11$  ns between the front row and back row signals. The multi-hit TDC used to instrument the FP array is the CAEN V1190B. The V1190B is a 64 channel device with 19 bit resolution. Once triggered, it uses one of the FP channel signals as the timing reference signal<sup>3</sup>. The module was programmed to accept up to 4 stop signals per channel for each trigger<sup>4</sup>. It was experimentally determined that these stop signals also had to be at least  $\sim 11$  ns in width. The device labeled scaler in Figs. 1 and 3 is a CAEN V830 scaler. The V830 is a 32 channel latching device with a 250 MHz counting capability. It was experimentally determined to register pulses a short as  $\sim 3$  ns in width, the limit of our FP-trigger setup.

<sup>3</sup> see <http://www.caen.it/csite/CaenProd.jsp?idmod=787&parent=11> for details

<sup>4</sup> In order to address the rate-dependent stolen-coincidence effect (see Sect. 3.3), a record of the first 2 signals presented by a FP channel is sufficient. We record the first 4 signals in order to be able to better confirm that our instrumentation electronics are behaving as expected.

Table 1: A summary of corrections to the number of tagged events registered by the FP array required for the absolute normalization of experimental data. Note that the stolen-coincidences correction is unnecessary when multi-hit TDCs are used, a distinct advantage. See text for details.

Correction	single-hit TDCs	multi-hit TDCs
Ghost events	1%	1%
Missed stops	3%	3%
Stolen coincidences	40%	N/A

Two advantages to requiring a coincidence between the front and back rows of electron detectors in the FP array are that registration of the background in the experimental hall is greatly suppressed, and that the photon-energy resolution may be easily increased simply by offsetting the two scintillator planes.

### 3. Rate-dependent effects

As the electron beam has a varying periodic intensity, high instantaneous post-bremsstrahlung electron event rates can occur. The resulting rate-dependent effects may result in significant losses in the number of events registered by the FP array instrumentation. Unless taken carefully into consideration, these rate-dependent effects prevent the absolute normalization of the experimental data. Rate-dependent effects include ghost events, missed stops, and stolen coincidences (see below). Table 1 summarizes typical values for rate-dependent corrections to the number of post-bremsstrahlung electrons detected by the FP array for both the single-hit and multi-hit TDCs.

#### 3.1. Ghost events

A major disadvantage of requiring a coincidence between the front and back rows of electron detectors in the FP array is the creation of ghost events at high rates. The ghost events result from the instrumentation of the FP array. The scenario leading to a ghost event is illustrated in Fig. 4. Two different post-bremsstrahlung electrons strike next-to-neighboring channels (counters F1 · B1 and F2 · B2) at nearly the same time which creates the illusion of an electron in the channel in between (counters F1 · B2) – the ghost event. The rate of the accidental coincidences that result in ghost events depends on the post-bremsstrahlung electron rate, the widths of the FP discriminator output pulses, and the resolving time of the overlap coincidence modules. Because these ghosts are formed in the FP electronics, they are registered as coincidences in both the FP scalers and the FP TDC modules, resulting in a partial but not complete cancellation of the effect. As the rate of ghost events is purely a function of post-bremsstrahlung electron rate and FP geometry, they affect both single-hit and multi-hit TDC data equally. They are best addressed using the simulation approach detailed in Ref. [4].

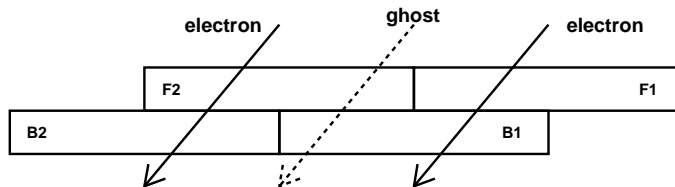


Figure 4: Creation of a ghost event. Real post-bremsstrahlung electrons (solid arrows) in next-to-neighboring FP channels arrive at almost the same time. This creates the illusion – or ghost – of an electron (dashed arrows) in the counters that constitute the intermediate FP channel. Figure from [4].

### 3.2. Missed stops

A missed stop occurs when the FP scalers register a recoil-electron event while the FP TDCs miss it. The primary origin of missed stops lies in the different minimum pulse width for registration in the FP scalers ( $\sim 3$  ns) and TDCs ( $\sim 11$  ns). This deadtime effect is best addressed using the simulation approach detailed in Ref. [4].

### 3.3. Stolen coincidences

When single-hit TDCs are employed, due to the fact that the TDC only registers the first signal presented to it subsequent to the start, an accidental post-bremsstrahlung electron may be detected in the FP channel before the actual post-bremsstrahlung electron that corresponds to the tagged photon. The result is that the single-hit TDC is stopped too early, leading to a well-studied phenomenon known as stolen coincidences – see Fig. 5. Well-known methods [12, 13] exist for determining the stolen-coincidence correction. It may also be efficiently addressed using the simulation approach detailed in Ref. [4] or greatly reduced by implementing multi-hit TDCs.

As previously mentioned, the multi-hit TDC with which the FP has been upgraded has been programmed to accept the first 4 stop signals presented to it in conjunction with the trigger and the programmable acceptance window. In this manner, the stolen-coincidence effect is greatly reduced as up to 3 accidental post-bremsstrahlung electrons can be registered in the multi-hit TDC before the prompt electron without stealing it. Thus, a large correction to the number of tagged events registered by the FP array is avoided, increasing the precision of the overall normalization.

The causes of ghost events, missed stops, stolen coincidences, and deadtime in the FP scalers and TDCs are all included in the FP simulation [4] which can therefore be used to determine suitable correction factors.

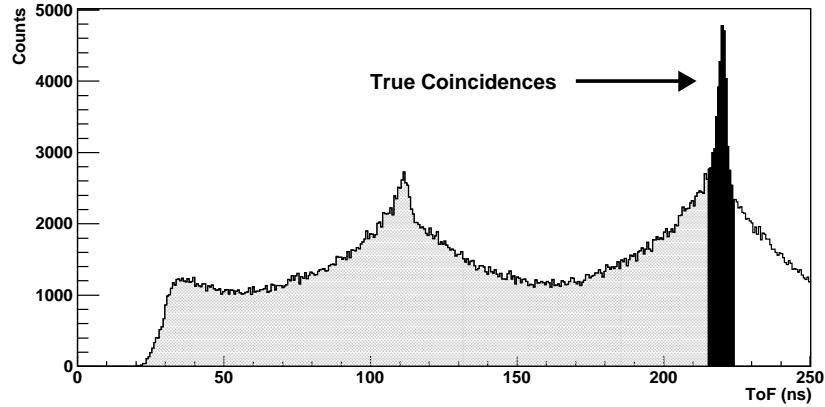


Figure 5: The stolen-coincidence effect in a single-hit TDC spectrum acquired at a high post-bremsstrahlung electron rate. The black peak at channel 225 represents true coincidences between the reaction-product detector and the FP array, and is the earliest possible time that a true coincidence may be registered. Events in the lightly shaded region correspond to accidental post-bremsstrahlung electrons that stop the FP TDCs before this earliest possible point in time. The coincidence is thus mis-timed and the true coincidence event is stolen when a single-hit TDC is used. Note that the “peak” at channel 110 is an artifact of the extracted electron beam. Figure from [4].

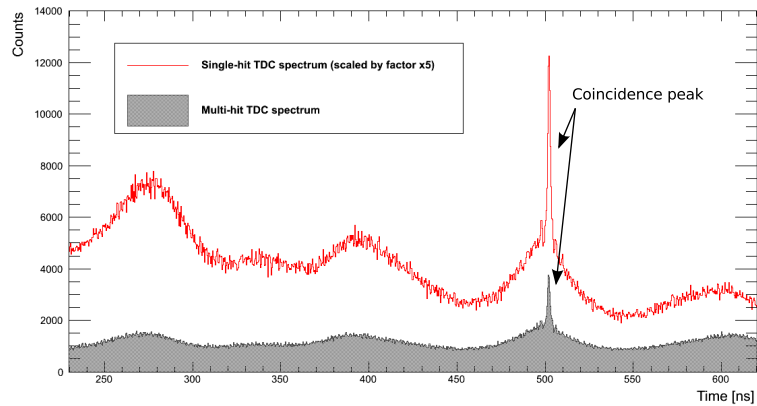


Figure 6: A comparison between single-hit (red, unshaded) and multi-hit (gray, shaded) FP TDC spectra obtained simultaneously. Note the  $\times 5$  scaling of the single-hit TDC spectrum. The time structure in the spectra is due to the method by which the beam is generated. The peak representing coincidences between the FP and the reaction-product detector is clearly evident at  $\sim 500$  ns. The slope of the background in the unshaded single-hit TDC spectrum is proportional to the post-bremsstrahlung electron rate and also to the magnitude of the stolen-coincidence correction. As expected, no slope is evident in the background in the shaded multi-hit TDC spectrum as coincidences may not be stolen. (For interpretation of the references to color in this figure caption, the reader is referred to the web version of this article.)

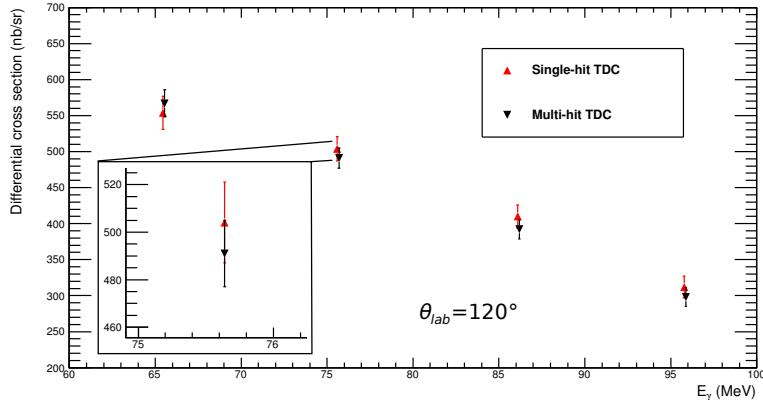


Figure 7: Absolute differential cross-section data for elastic photon scattering from  $^{12}\text{C}$  at a lab angle of  $120^\circ$  obtained simultaneously using both single-hit (upright red triangles) and multi-hit (inverted black triangles) TDCs. The single-hit TDC data have been corrected according to Ref. [4]. Statistical uncertainties only are shown. See text for details. (For interpretation of the references to color in this figure caption, the reader is referred to the web version of this article.)

#### 4. Results

Figure 7 presents a comparison between the absolute differential cross section for elastic photon scattering from  $^{12}\text{C}$  at a lab angle of  $120^\circ$  recently obtained at the TPF at the MAX IV Laboratory using both single-hit (upright red triangles) and multi-hit TDCs (inverted black triangles) simultaneously. The single-hit TDC data have been corrected for stolen coincidences according to Ref. [4]. Error bars reflect statistical uncertainties only. The agreement between the two data sets is satisfactory, thereby confirming our understanding of the stolen-coincidence correction to the data.

Figure 8 presents a comparison between the absolute differential cross section for elastic photon scattering from  $^{12}\text{C}$  at a lab angle of  $120^\circ$  recently obtained at the TPF at the MAX IV Laboratory and existing data published by Schelhaas *et al.* [14] (open upright triangles) and Warkentin *et al.* [15] (open squares). Error bars reflect statistical uncertainties only. Systematic uncertainty bands for the present measurement are presented at the top (red, single-hit TDC data) and bottom (gray, multi-hit TDC data) of the figure. The agreement between the data sets is very good thereby confirming our understanding of the absolute normalization.

#### 5. Summary

In this paper, the Monte Carlo simulation [4] of the MAX IV tagger focal-plane electronics has been tested by comparing results obtained using both



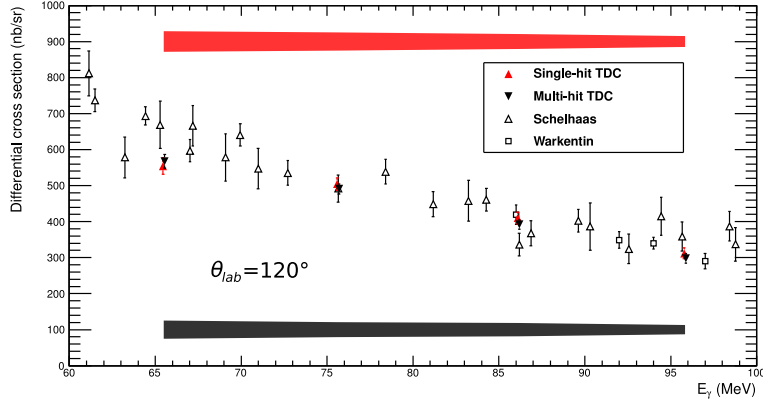


Figure 8: Absolute differential cross-section data for elastic photon scattering from  $^{12}\text{C}$  at a lab angle of  $120^\circ$  obtained simultaneously using both single-hit (upright red triangles) and multi-hit (inverted black triangles) TDCs compared to published data. The single-hit TDC data have been corrected according to Ref. [4]. Statistical uncertainties only are shown. Systematic uncertainty bands for the present measurement are presented at the top (corrected single-hit TDC data) and bottom (multi-hit TDC data) of the figure. See text for details. (For interpretation of the references to color in this figure caption, the reader is referred to the web version of this article.)

single- and multi-hit TDCs. Good agreement between these data sets has been demonstrated, and the measured absolute cross sections also agree with previous experiments. We conclude that the behavior of the detector system is thoroughly understood and that the Monte Carlo simulation incorporates it correctly.

## Acknowledgements

This project was supported by the US National Science Foundation Grant No. 0855569, the UK Science and Technology Facilities Council, as well as The Swedish Research Council, the Crafoord Foundation, and the Royal Physiographic Society in Lund. The authors gratefully acknowledge the Data Management and Software Centre, a Danish Contribution to the European Spallation Source ESS AB, for generously providing access to their computations cluster. We also thank J.C. McGeorge for useful discussions.

## References

- [1] J.-O. Adler, M. Boland, J. Brudvik, K. Fissum, K. Hansen, L. Isaksson, P. Lilja, L.-J. Lindgren, M. Lundin, B. Nilsson, D. Pugachov, A. Sandell, B. Schröder, V. Avdeichikov, P. Golubev, B. Jakobsson, J.R.M. Annand, K. Livingston, R. Igarashi, L. Myers, A. Nathan, W.J. Briscoe, G. Feldman, M. Kovash, D. Branford, K. Föhl, P. Grabmayr, V. Takau, G. O’Rielly,

- D. Burdeynyi, V. Ganenko, V. Morochovskyi, G. Vashchenko, Nucl. Instrum. and Meth. A 715 (2013) 1.
- [2] <https://www.maxlab.lu.se/node/1090>
- [3] <https://www.maxlab.lu.se>
- [4] L.S. Myers, G. Feldman, K.G. Fissum, L. Isaksson, M.A. Kovash, A.M. Nathan, R.E. Pywell, B. Schröder, Nucl. Instr. and Meth. A 729 (2013) 707.
- [5] for example L.S. Myers *et al.*, to be submitted to Phys. Rev. C in 2013.
- [6] J.M. Vogt, R.E. Pywell, D.M. Skopik, E.L. Hallin, J.C. Bergstrom, H.S. Caplan, K.I. Blomqvist, W. Del Bianco, J.W. Jury, Nucl. Instrum. and Meth. A 324 (1993) 198.
- [7] Annual Report 1994, Saskatchewan Accelerator Laboratory, p. 21-23.
- [8] Annual Report 1995, Saskatchewan Accelerator Laboratory, p. 27-29.
- [9] see for example J.-O. Adler, B.-E. Andersson, K.I. Blomqvist, B. Forkman, K. Hansen, L. Isaksson, K. Lindgren, D. Nilsson, A. Sandell, B. Schröder, K. Ziakas, Nucl. Instr. and Meth. A 294 (1990) 15.
- [10] see for example J.-O. Adler, B.-E. Andersson, K.I. Blomqvist, K.G. Fissum, K. Hansen, L. Isaksson, B. Nilsson, D. Nilsson, H. Ruijter, A. Sandell, B. Schröder, D.A. Sims, Nucl. Instr. and Meth. A 388 (1997) 17.
- [11] L.-J. Lindgren, Nucl. Instrum. and Meth. A 492 (2002) 299.
- [12] R.O. Owens, Nucl. Instr. and Meth. A 288 (1990) 574.
- [13] L. Van Hoorebeke, D. Ryckbosch, C. Van den Abeele, R. Van de Vyver, J. Dias, F. De Smet, B. Schröder, D. Nilsson Nucl. Instr. and Meth. A 321 (1992) 230.
- [14] K.P. Schelhaas, J.M. Henneberg, N. Wieloch-Laufenberg, U. Zurmühl, B. Ziegler, M. Schumacher, F. Wolf, Nucl. Phys. A 506 (1990) 307.
- [15] B.J. Warkentin, D.L. Hornidge, R. Igarashi, J.C. Bergstrom, E.L. Hallin, N.R. Kolb, R.E. Pywell, D.M. Skopik, J.M. Vogt, G. Feldman Phys. Rev. C 64 (2001) 014603.